IEEE Access
Multidisciplinary | Rapid Review | Open Access Journal

Received 16 July 2024, accepted 3 August 2024, date of publication 13 August 2024, date of current version 23 August 2024.

Digital Object Identifier 10.1109/ACCESS.2024.3442890

RESEARCH ARTICLE

5.58-GHz Modified Jerusalem Patch Sensor for 1%-Precision Ethanol and Methanol Discrimination in Disinfectant Solutions

NONCHANUTT CHUDPOOTI[1], (Member, IEEE), TANAPORN PECHRKOOL[2], PATCHADAPORN SANGPET[2], PRAYOOT AKKARAEKTHALIN[2], (Member, IEEE), IAN D. ROBERTSON[3], (Fellow, IEEE), AND NUTAPONG SOMJIT[3,4,5], (Senior Member, IEEE)

[1]Department of Industrial Physics and Medical Instrumentation, Faculty of Applied Science, King Mongkut's University of Technology North Bangkok, Bangkok 10800, Thailand
[2]Department of Electrical and Computer Engineering, Faculty of Engineering, King Mongkut's University of Technology North Bangkok, Bangkok 10800, Thailand
[3]School of Electronic and Electrical Engineering, University of Leeds, LS2 9JT Leeds, U.K.
[4]Department of Mathematical and Information Sciences, Shaoxing University, Shaoxing 312000, China
[5]Division of Micro and Nanosystems (MST), KTH Royal Institute of Technology, SE-100 44 Stockholm, Sweden

Corresponding author: Nutapong Somjit (n.somjit@leeds.ac.uk)

This work was supported in part by the National Science, Research and Innovation Fund (NSRF), and King Mongkut's University of Technology North Bangkok, under Contract KMUTNB-FF-66-49; in part by the Engineering and Physical Science Research Council under Grant EP/S016813/1; and in part by Swedish Research Council (VR) under Grant 2021-05842_VR.

ABSTRACT This paper presents a state-of-the-art planar microwave sensor designed for highly precise alcohol characterization in aqueous solutions, with a primary focus on its application in COVID-19 disinfectants. Modified from the Jerusalem patch, the sensor operates at 5.58 GHz, achieving a unique balance between heightened sensitivity and cost-effectiveness. A tailor-made 3D-printed case minimizes errors, securely housing the sensor and feeding tube. The sensor effectively discriminates between ethanol and methanol, revealing a notable 16 MHz frequency gap. In COVID-19 applications, it maintains alcohol percentages at 65–75%, with 1% increments. The paper outlines a mathematical model extracting concentrations with the maximum error of only smaller than 1.81%, affirming the sensor's precision. Beyond technical prowess, the sensor's non-destructive nature, real-time monitoring applicability, and freedom from life-cycle limitations mark it as an innovative tool for checking the percentage of alcohol and types of alcohol before using it to kill the virus, contributing significantly to global efforts on disinfectant measurements with noninvasive nature and high precision. This modified Jerusalem sensor stands as a transformative solution, offering unprecedented advantages in design, operational capacity, and broader support for virus-killing applications.

INDEX TERMS Modified Jerusalem resonator, microwave sensor, non-destructive method, alcohol–aqueous solution, disinfectants against COVID-19.

I. INTRODUCTION

The emergence of the 2019 Coronavirus Disease (COVID-19) in December 2019 has precipitated a global pandemic with staggering implications, marked by over 6.9 million fatalities as of July 2022 [1]. This stark reality underscores the pressing need for innovative solutions to counteract the rapid spread of viruses, emphasizing the critical importance of a comprehensive understanding of their pathogenesis and modes of transmission. In [2] and [3], research demonstrates the effectiveness of killing the coronavirus by using disinfectants with an alcohol percentage of at least 60%. However, higher concentrations of alcohol are more effective in killing the virus but can have adverse effects on human skin when the concentration exceeds 80% [4], [5]. Despite the instrumental role of alcohol-based disinfectants, challenges persist in

The associate editor coordinating the review of this manuscript and approving it for publication was Patrizia Livreri.

accurately determining ethanol percentage and differentiating between alcohol types in disinfectant solutions. The need for precise characterization in alcohol-based solutions is crucial not only for combating the ongoing COVID-19 pandemic but also for addressing potential future viral threats. Existing methods often fall short in providing a comprehensive solution, leaving a notable research gap that our work seeks to fill.

In response to these challenges, this paper introduces a pioneering planar microwave sensor designed explicitly for evaluating alcohol type and concentration in aqueous solutions. This innovation is not only timely in the context of the ongoing pandemic but also addresses a broader need for advanced sensing technologies to combat various viruses. The proposed sensor allows for detecting disinfectant solutions in two modes: identifying the type of alcohol and determining the percentage of alcohol. This approach offers benefits for bacterial and viral eradication purposes, which can significantly aid in pandemic preparedness efforts both presently and in the future.

Microwave and millimeter-wave sensors, known for their versatility in distinguishing between different material categories [6], [7], [8], [9], [10], [11], [12], [13], [14], [15], [16], [17], [18], [19], [20], [21], [22], [23], [24], [25], [26], [27], [28], [29], [30], [31], [32], [33], [34], [35], [36], [37], [38], have become crucial components in the arsenal against viral spread. While resonance methods have traditionally been applied to solid material characterization, [11], [12], [22], [24] recent advancements have demonstrated their effectiveness in detecting and quantifying liquid materials [11], [13], [14], [15], [17], [18], [22], [24], [35], [37]. Meanwhile, transmission-line methods, offering a broader bandwidth, have been successfully employed in characterizing both liquids and solids [10], [19], [20], [21], [27], [28], [29], [30], [31], [32], [33], [34], [39], [40]. Nevertheless, liquid measurements with resonance methods are hindered by high-loss materials, impacting measurement accuracy [32], [33], [34], [36].

To specify the characterization of liquid properties, such as the type of liquid and its concentration, various structures have been developed for use in numerous applications. In [11], [14], and [17], the published sensors operating at a single resonance frequency reported a technique for detecting glucose concentration with noninvasive capabilities. Furthermore, an investigation into the dual-frequency technique for detecting liquid samples was conducted [11], [12].

The unique contribution of our work lies in the application of a modified Jerusalem patch to enhance the electrical field's strength and reduce physical dimensions in the planar microwave sensor. Operating at 5.58 GHz, this sensor strikes an optimal balance between sensitivity and development costs, making it a practical and cost-effective solution. The integration of 3D printing technology for casing fabrication further enhances the sensor's capabilities, ensuring a secure enclosure and minimizing potential measurement errors.

The experimental results underscore the ground-breaking capability of the sensor to differentiate between ethanol and methanol in aqueous solutions, presenting a notable frequency gap of 16 MHz between the two alcohols. Significantly, the sensor accurately classifies alcohol types within the 65–75% concentration range with 1% increments. The mathematical model constructed from these results attains an exceptional accuracy exceeding 98.19% when compared to extraction models and alcohol percentages in both ethanol and methanol solutions, including water.

This modified Jerusalem sensor stands out as a significant advancement in alcohol sensing technology, offering a non-destructive nature, applicability in real-time monitoring systems, and freedom from life-cycle limitations. Beyond its immediate application in disinfectants against COVID-19, the sensor's versatility positions it as a pivotal innovation in the ongoing global efforts to combat a spectrum of viruses [4]. By addressing the existing research gaps and offering a comprehensive solution, our work significantly contributes to advancing the field of checking the percentage of alcohol before using it to kill the virus and mitigation strategies. The key advantages of the proposed sensor lie in its ability to combine: (1) non-destructive measurements, which allow for testing without causing harm, alteration, or damage to the sample under test; (2) freedom from life-cycle limitations, as the sensor operates consistently and reliably throughout its intended lifespan without degradation from normal environmental conditions; and (3) noninvasive data collection, enabling measurements without physically penetrating or causing harm to the sample under test.

II. DESIGN AND FABRICATION

A. WORKING PRINCIPLE

The working principle of the proposed sensor relies on a one-port measurement, involving the reflected and radiated interaction between the electromagnetic (EM) wave emitted from the top of the Jerusalem resonator and the liquid sample under test. To detect changes in the type and percentage of alcohol in the liquid mixture, the resonant peak is monitored and collected to generate the extraction function. The change in resonant frequency is directly associated with the variation in the system's capacitance, which occurs due to the differing electrical properties of the liquid under test.

To investigate the equivalent circuit model of the Jerusalem liquid sensor, in [11], [16], and [41]. Due to the complicated structure of the folded line in the Jerusalem's sleeve,

Figure 1(a) depicts the aggregation of the equivalent circuit model of the Jerusalem sensor with the loading of the Teflon tube and liquid sample. To validate the equivalent circuit model, figure 1(b) shows the comparison of the reflection coefficient, S_{11}, of the resonator between the 3D EM analysis of the Jerusalem resonator at the operating frequency of 5.58 GHz and the optimized value in the equivalent circuit mode using Microwave Studio (CST MWS) [42]. The terms R_R, L_R, and C_R denote the collective summation of

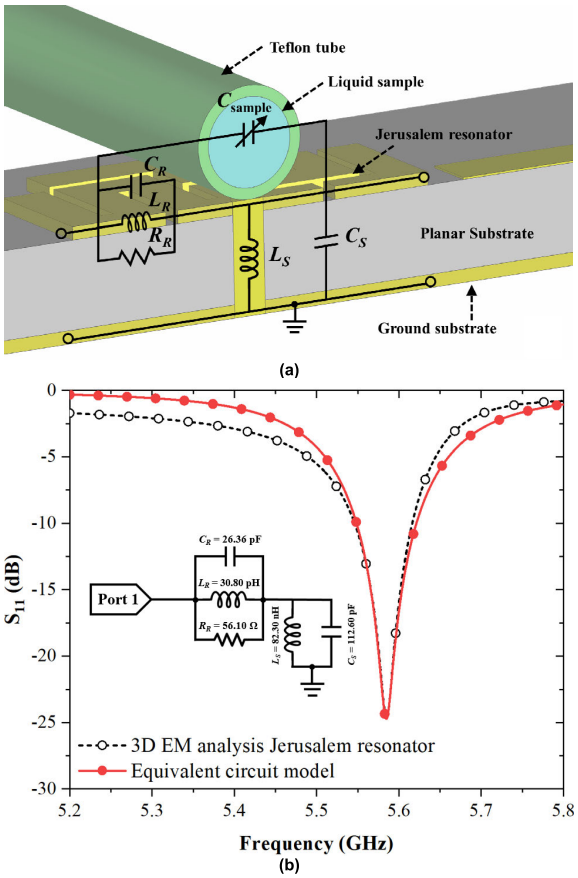

FIGURE 1. Equivalent circuit model of (a) the Jerusalem resonator and (b) the Jerusalem sensor with loading of the Teflon tube and liquid sample.

the resistance, inductance, and capacitance of the Jerusalem model, respectively. The capacitance, C_S, signifies the dielectric substrate gap between the resonator and ground. The shunt inductor, L_S, represents the inductances of the vias, which are connected from the resonator to the ground. The resonant frequency of the Jerusalem resonator is designed and calculated using Eq. (1) [43]:

$$f_r = \frac{1}{2\pi\sqrt{C_{Total} \cdot L_{Total}}} \tag{1}$$

where the C_{Total} and L_{Total} represent the summation of the capacitance and inductance of the equivalent circuit model. When the liquid sample fills in the Teflon tube, the capacitance of the liquid sample, denoted as C_{sample} and calculated using Eq. (2) as follow:

$$f_{r(sample\ loading)} = \frac{1}{2\pi\sqrt{C_{Total} \parallel C_{sample} \cdot L_{Total}}} \tag{2}$$

The capacitance of the sample, C_{sample} will also change, resulting in a decrease in the resonant frequency shift. Consequently, the observed resonant frequency shift provides data for creating the extraction function, aiding in the classification of both the type and percentage of alcohol present in the liquid mixture.

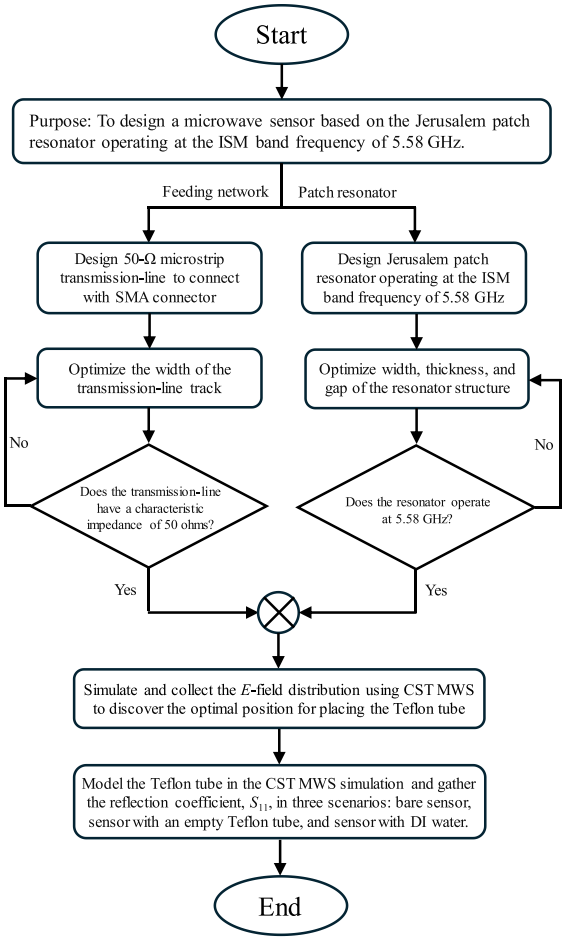

FIGURE 2. Flowchart of the proposed sensor design.

B. DESIGN OF THE MODIFIED JERUSALEM LIQUID MIXTURE SENSOR

The proposed sensor was designed to be planar-based for ease of fabrication and future embedding with other circuits. Due to its low-loss properties, an RT/Duroid 5880 [44] was selected to design the sensor. The substrate's relative permittivity, ε_r, and loss tangent, $tan\delta$, were 2.2 and 0.0009, respectively. The thickness of the substrate was 1.575 mm. Designing a Jerusalem resonator on the substrate without a sample placed on top (i.e., the resonator remains unloaded by the liquid sample) results in the observation of reflection coefficient, S_{11}, at the nominal resonant frequency of 5.58 GHz. This operating frequency resonates within the Industrial, Scientific and Medical (ISM) band, showcasing a good compromise between sensitivity and development costs. Lower frequencies entail lower fabrication costs but compromised sensitivity. Conversely, higher frequencies offer improved sensitivity but come with increased overall process costs. Figure 2 depicts the design flowchart [45] of the modified Jerusalem liquid mixture sensor. The sensor was developed using a modified Jerusalem patch to increase the electrical field's strength and reduce its physical dimensions [46], [47], [48]. Each branch of the Jerusalem structure has an

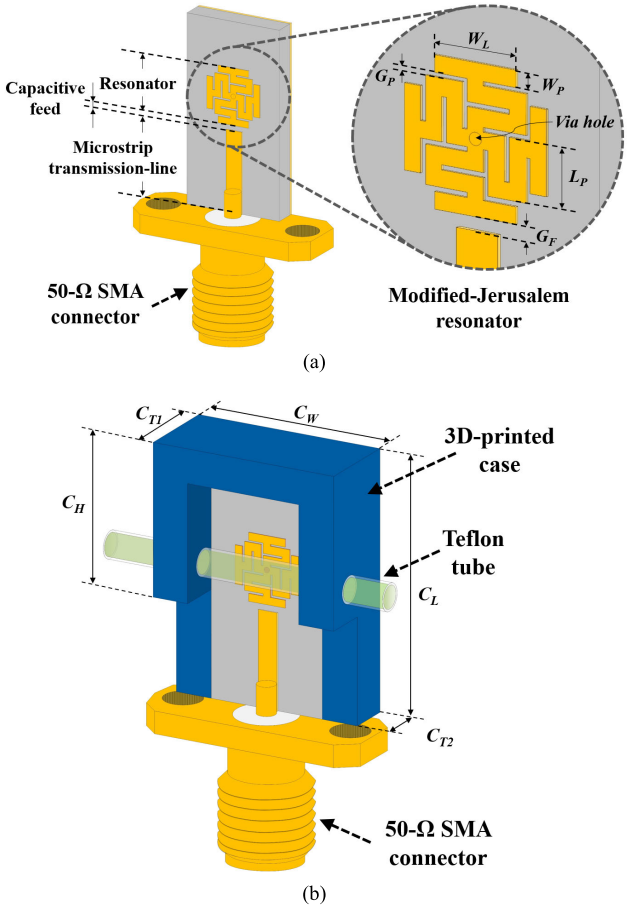

FIGURE 3. 3D view of the sensor: (a) modified Jerusalem resonator and (b) the modified Jerusalem resonator integrated with a 3D-printed case.

electrical length equivalent to λ/4. The Jerusalem branch is folded with a mushroom-like structure and connected to the ground through vias with a diameter of 0.6 mm to reduce the size further and confine the electrical field (*E*-field). Using a capacitive feed technique, the sensor is fed by a 50-Ω microstrip transmission-line.

A 50-Ω SubMiniature version A (SMA) connector is attached at the end of the transmission-line for interfacing with the vector network analyzer (VNA) signal. Figure 3(a) shows the perspective view of the modified Jerusalem sensor, and Table 1 provides the key parameters essential for designing this sensor. The parameter values were optimized using Microwave Studio (CST MWS) for operation at 5.58 GHz.

CST MWS was used to simulate the *E*-field strength at the operating frequency to investigate the best practice area for placing the liquid sample tube. Figure 4 shows the *E*-field distribution at 5.58 GHz, resulting in the maximum *E*-field of 29,688 V/m around the four edges of the modified Jerusalem resonator. The red areas are good candidates for sensing the liquid sample. Thus, the EM fields will disturb the liquid being tested, affecting the reflection coefficient change in resonance frequency. Therefore, a Teflon tube was chosen and placed across the modified Jerusalem patch to feed the liquid sample for testing, as shown in Figure 3(b).

TABLE 1. Key parameters of the modified Jerusalem sensor.

Parameters	Descriptions	Optimized values (mm)
W_L	Width of the resonator structure	7
W_P	Thickness of the resonator structure	0.8
L_P	Length of the resonator structure	2.9
G_P	Gap of the resonator structure	0.25
G_F	Gap of the capacitive feed	0.33
Via hole	Diameter of vias	0.6

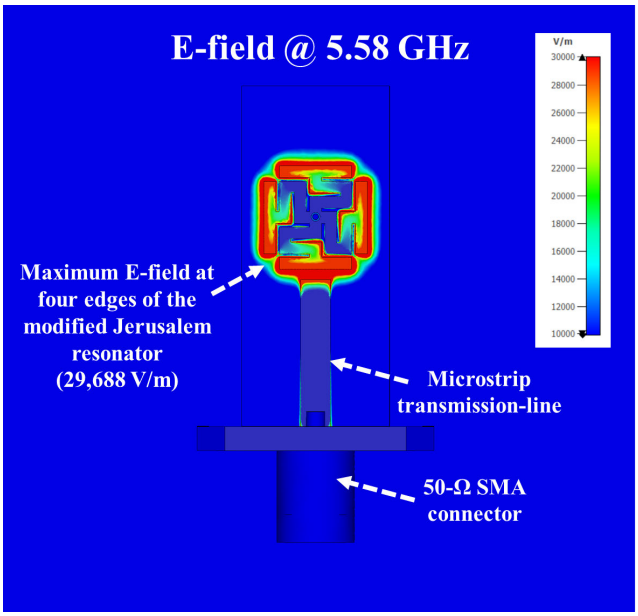

FIGURE 4. Simulated E-field distribution of the bare modified Jerusalem sensor at an operating frequency of 5.58 GHz.

Figure 3(b) displays the 3D perspective view of the modified Jerusalem sensor integrated with the 3D-printed case, with the Teflon tube inserted across the Jerusalem patch. The inner and outer diameters of the Teflon tube are 2 mm and 3 mm, respectively. The purpose of the 3D-printed case is to secure the position of the Teflon tube during measurement, reducing the impact of realignment and re-measurement. The design of the 3D-printed case was tailored to fit the modified Jerusalem sensor. It has a width, C_W, of 20 mm and a length, C_L, of 23.5 mm. The case thickness is divided into two sections: the transmission-line section and the resonator section. In the resonator section, the thickness of the 3D-printed case, C_{T1}, is 9.5 mm to accommodate the creation of a hole for locking the Teflon tube. The length of this section of the 3D-printed case, C_H, measures 12.2 mm. In the transmission-line section, the 3D-printed case, C_{T2}, is 5 mm thick.

C. FABRICATION OF THE MODIFIED JERUSALEM LIQUID MIXTURE SENSOR

The methods were divided into two components to fabricate all sensor parts: the modified Jerusalem resonator and the

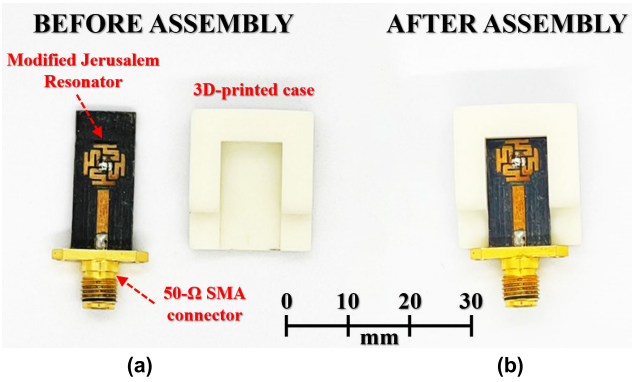

FIGURE 5. Fabricated part of the proposed sensor, including the modified Jerusalem resonator and 3D-printed case (a) before assembly and (b) after assembly.

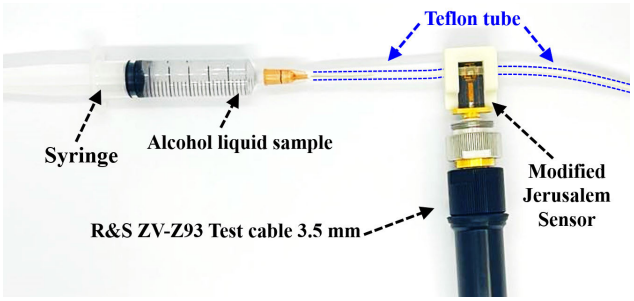

FIGURE 6. Measurement setup for the system for testing alcohol in aqueous solutions.

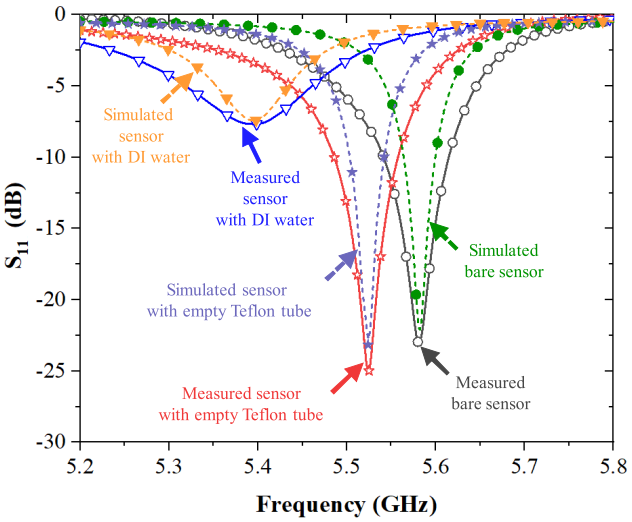

FIGURE 7. Reflection coefficient, S_{11}, comparing between the simulation and measurement for three cases: bare sensor, sensor with the empty Teflon tube, and sensor with DI water.

3D-printed case. The modified Jerusalem resonator was first exported from the CST MWS using the DXF file format. The top and bottom views of the resonator were routed and fabricated using an LPKF Protomat S100 circuit board plotter [49]. Then, the 0.6-mm drilling at the center of the Jerusalem resonator was used to insert the vias hole via a 0.6-mm-diameter wire to connect the patch and ground. When finished with the LPKF Protomat S100, the fabricated resonator was connected with a 50-ohm SMA connector at the end of the transmission-line.

Second, the 3D-printed case was built using the digital light processing (DLP) technique to ensure the case's precision fit the fabricated sensor. The 3D-printed case model was exported from the CST MWS using the STL file format. The Anycubic Photon Ultra [50] was the printing machine used to fabricate the 3D-printed case. The printing parameters were set with a printing resolution of 0.050 mm and an exposure time of 2.0 second. The resin is a 3D-printed UV-sensitive resin with a UV wavelength of 405 nm [51] and a white color. When printing was finished, the 3D-printed case was cleaned and cured for 20 minutes during each process. Figure 5 shows the fabricated resonator and fabricated 3D-printed case (a) before and (b) after assembly.

III. MEASUREMENT RESULTS

A. MEASUREMENT SETUP AND INITIAL RESULTS

The goal of the proposed sensor concept was to measure the changes in response parameters, such as frequency and magnitude, during one-port measurements by injecting a sample into the Teflon tube. The Rohde & Schwarz ZVB-20 VNA was employed for the one-port measurements. To mitigate noise and signal loss within the coaxial line and SMA connector, The open–short–match (OSM) technique was used to calibrate all signals. For the parameter configuration in VNA, the active frequency range was set from 5 to 6 GHz with 10,001 measurement points and an intermediate frequency (IF) bandwidth of 10 Hz.

The fabricated sensor was linked to the VNA to test the prototype sensor via the sample measurement. A torque of 0.9 Nm was applied to establish a secure connection between the SMA port and the coaxial line, minimizing connectivity effects. Three scenarios were examined: the bare sensor, the sensor with an empty channel Teflon tube, and the sensor with deionized water (DI). A precise approach was used to introduce the sample solution into the Teflon tube using a high-quality industrial syringe, ensuring the absence of air bubbles in the liquid path. The sample temperature was maintained at a constant room temperature of 25°C. Figure 6 shows the measurement setup of the proposed sensor upon connecting it to the VNA and inserting the syringe.

Figure 7 compares the reflection coefficient, S_{11}, between the simulation and measurement for the three cases: bare sensor, sensor with the empty Teflon tube, and sensor with DI water. In the simulation, the existing materials available in the CST MWS software were selected. Specifically, two materials were chosen: water (Debye Model) and PTFE. The water (Debye Model) was employed as a substitute for DI water, utilizing first-order dispersion with an epsilon infinity of 3.1, an epsilon static of 78.4, and relaxation times of 8.27×10^{-12}. Additionally, PTFE was used to substitute the Teflon tube, with a relative permittivity of 2.1 and a

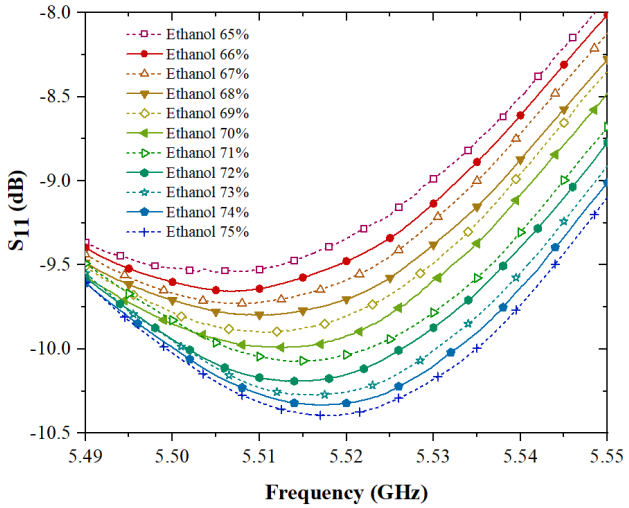

FIGURE 8. Measured results of the reflection coefficient, S_{11}, response upon varying the ethanol concentration from 65 to 75% in aqueous solutions.

loss tangent of 0.0002. The results showed a high degree of accuracy between the compared datasets. According to the results, the bare sensor's reflection coefficient, S_{11}, resonated at 5.586 GHz with a magnitude of −22.64 dB. The fully assembled sensor without a sample (air, $\varepsilon_r = 1$) resonated at 5.512 GHz with a magnitude of −25.18 dB. When DI water was injected ($\varepsilon_r = 78$), the resonant frequency shifted to 5.406 GHz with a magnitude of −7.74 dB. The frequency variation of 106 MHz between sensors with and without DI water suggests that altering the dielectric constant from 1 to 78 results in a 106 MHz frequency shift. This indicates that the sensor resolution can be computed using Eq. (3) as follows:

$$\text{Sensor Resolution} = \frac{\Delta \text{ resonant frequency}}{\Delta \varepsilon_r} \tag{3}$$

Consequently, the proposed sensor's resolution is 1.37 MHz per unit of dielectric constant.

B. ETHANOL-AQUEOUS SOLUTION CHARACTERIZATION

The first set of solutions investigated involved ethanol. Eleven concentration solutions, ranging from 65% to 75% ethanol with a 1% increment, were analyzed to determine the reflection coefficient, S_{11}, responses. For each sample solution, the coefficient was recorded three times to ensure the repeatability of the sensor measurements. Figure 8 shows the S_{11} results obtained from these eleven solutions with DI water. The average resonant frequencies are provided in Table 2.

To establish the frequency relationship related to the ethanol percentage in aqueous solutions, eleven concentration solutions, ranging from 65% to 75%, along with DI water, are chosen. A linear fitting is applied to predict the model. Figure 9 shows this linear fitting, with the resonant frequency on the x-axis and the ethanol concentration in the aqueous solutions on the y-axis. The linear fitting equation takes the form:

$$E_c(\%) = 659.98 f_r(GHz) - 3,567.95 \tag{4}$$

In this equation, E_c represents the percentage of ethanol in the aqueous solution, and f_r corresponds to the resonant frequency of the measurement unit in GHz.

To evaluate the uncertainty of the linear fitting equation, The authors listed the inferred ethanol concentrations in aqueous solutions and computed the maximum errors, as shown in Table 2. The maximum error for Eq. (4) was found to be 0.6896%, validating its suitability for categorizing the ethanol percentage in the aqueous solutions. However, the percentage error for the DI water cannot be calculated because the divisor is zero, resulting in the percentage error equation equaling infinity.

TABLE 2. Measured and extracted ethanol concentration in aqueous solutions between 65 and 75%.

Average resonant frequency (GHz)	Ethanol concentration	Extraction concentration from Eq. (4)	Absolute percentage error between the actual and Eq. (4)
5.4060	0%	0.098%	-
5.5050	65%	65.24%	0.3691
5.5065	66%	66.23%	0.3483
5.5078	67%	67.09%	0.1311
5.5095	68%	68.21%	0.3085
5.5109	69%	69.13%	0.1939
5.5125	70%	70.19%	0.2711
5.5140	71%	71.18%	0.2531
5.5153	72%	72.04%	0.0524
5.5164	73%	72.76%	0.3237
5.5175	74%	73.49%	0.6897
5.5191	75%	74.55%	0.6058

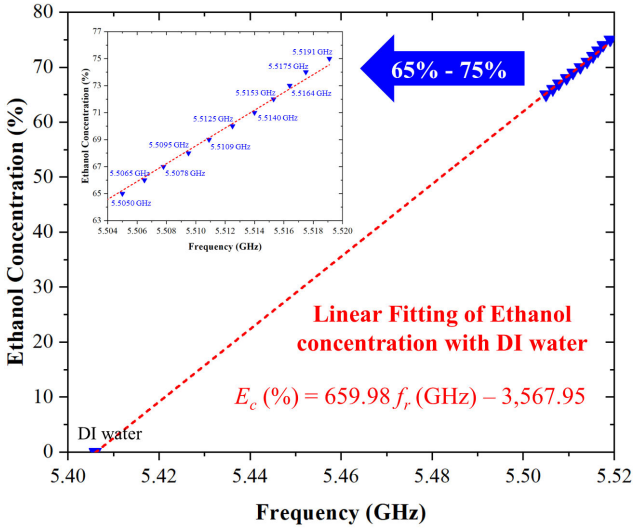

FIGURE 9. Linear fitting of the resonant frequency for predicting the percentage of ethanol in aqueous solutions.

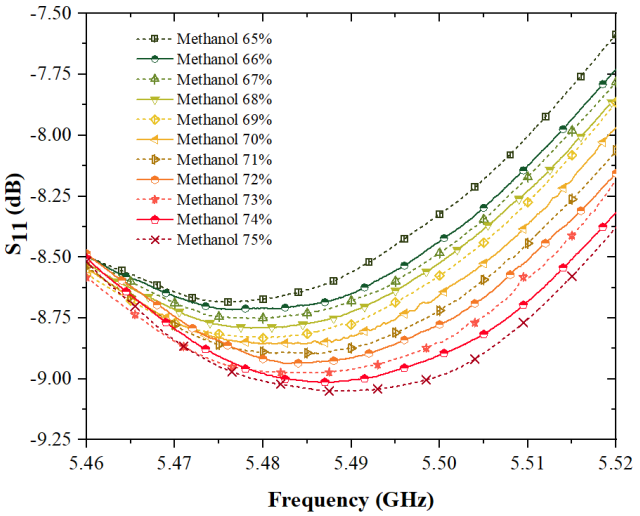

FIGURE 10. Measured reflection coefficient, S_{11}, response upon varying the methanol concentration from 65 to 75% in aqueous solutions.

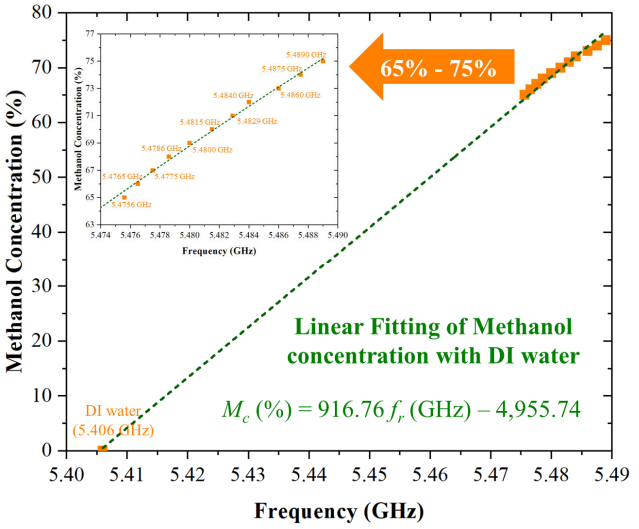

FIGURE 11. Linear fitting of the resonant frequency to predict the percentage of methanol in different aqueous solutions.

TABLE 3. Measured and extracted methanol concentrations in aqueous solutions between 65 and 75%.

Average resonant frequency (GHz)	Methanol concentration	Extraction concentration from Eq. (5)	Absolute percentage error between actual and Eq. (5)
5.4060	0%	0.265%	-
5.4756	65%	64.07%	1.4291
5.4765	66%	64.90%	1.6725
5.4775	67%	65.81%	1.7718
5.4786	68%	66.82%	1.7333
5.4800	69%	68.10%	1.2974
5.4815	70%	69.48%	0.7429
5.4829	71%	70.76%	0.3332
5.4840	72%	71.77%	0.3169
5.4860	73%	73.61%	0.8293
5.4875	74%	74.98%	1.3250
5.4890	75%	76.36%	1.8075

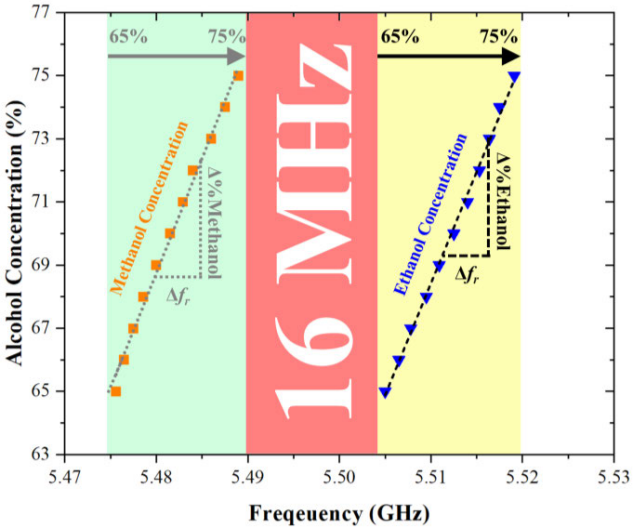

FIGURE 12. Sensitivity of the proposed sensor for detecting methanol and ethanol in aqueous solutions, as determined using a linear curve fitting approximation.

C. METHANOL-AQUEOUS SOLUTION CHARACTERIZATION

The second type of alcohol investigated was methanol. Eleven sample solutions were prepared, with the same range as for ethanol concentrations. Figure 10 shows the measured reflection coefficients, S_{11}, from eleven solutions. Table 3 shows the average resonant frequencies of eleven solutions with DI water. Figure 11 shows the linear fitting, with resonant frequency on the x-axis and methanol concentration in the aqueous solutions on the y-axis. Then, the linear fitting was used to classify the predicted equation. The linear fitting equation takes the form:

$$M_c(\%) = 916.76 f_r(GHz) - 4,955.74 \quad (5)$$

In this equation, M_c represents the percentage of methanol the in aqueous solution, and f_r corresponds to the resonant frequency in GHz.

To assess the level of uncertainty in the linear fitting equation, we recorded the derived methanol concentrations in the aqueous solutions, and the highest margin of error was calculated, as indicated in Table 3. The maximum error associated with Eq. (5) is 1.8075%.

D. ALCOHOL-AQUEOUS SOLUTION CLASSIFICATION

This section summarizes all the results, including ethanol and methanol concentrations in the aqueous solutions. Figure 11 shows the resonant points of 11 data points for ethanol and methanol. The measurement range of concentration is from 65 to 75%.

For methanol in the aqueous solutions, the lowest resonant frequency was observed at 5.4756 GHz, indicating lower methanol content. As the methanol concentration increased,

Table 4. Key factor comparison of the sensors in this work and from other works.

Ref.	Liquid Under Test (LUT)	Liquid Concentration	Topology	Sensor Materials	Reusable	Operating Frequency (GHz)	Maximum Sensing Bandwidth	Sensitivity (per % concentration)	*Q*-Factor	Frequency Detection Resolution (FDR) (GHz)	Maximum Measurement Error	Dimensions (mm)
[6]	Ethanol	0–100% step size of 10%	Complementary split-ring resonator (CSRR)	Rogers RT6002	No	2 GHz	400 MHz	4 MHz	N/A	0.0057	4.3%	$0.078\lambda_g \times 0.24\ \lambda_g$
[8]	Ethanol	0–5% step size of 1% 10–100% step size of 20%	Substrate-integrated waveguide (SIW)	Rogers RT/Duroid 5880	Yes	4.7 GHz	400 MHz	4 MHz	N/A	N/A	N/A	$0.81\ \lambda_g \times 0.93\ \lambda_g$
[9]	Methanol	0–100% step size of 10%	mu negative (MNG) metamaterial	Rogers RO3020	No	3.43 GHz	800 MHZ	8 MHz	N/A	0.1527	N/A	$0.023\ \lambda_g \times 0.023\ \lambda_g$
[13]	Ethanol	0%, 100%	Label-Free Meandered	Rogers RO4003	No	6.21 GHz	2.15 GHz	21.5 MHz	506	0.0398	2 %	$0.85\ \lambda_g \times 0.49\ \lambda_g$
	Methanol	0%, 100%					1.83 GHz	18.3 MHz		0.0398		
[15]	Ethanol	0%, 10%, 30%, 50%, 70%, 90%, 100%	Split ring resonator (SRR)	Rogers RO4003	No	CH_1 5.76 GHz CH_2 7.85 GHz	CH_1 850 MHz CH_2 1.21 GHz	CH_1 8.5 MHz CH_2 12.5 MHz	CH_1 280 CH_2 110	CH_1 0.016 CH_2 0.022	CH_1 0.52% CH_2 1.14%	$0.40\ \lambda_g \times 0.33\ \lambda_g$
[18]	Methanol	0–100% step size of 20%	Substrate-integrated waveguide (SIW)	Rogers RT/Duroid 5880	No	10 GHz	80 MHz	0.8 MHz	N/A	0.0014	2.93%	$1.13\ \lambda_g \times 0.64\ \lambda_g$
[19]	Ethanol	10–90% step size of 10%	Microstrip splitter/combiner with Split-ring resonator	Rogers RO3010	Yes	0.87 GHz	0.79 MHz	9.87 kHz	N/A	N/A	N/A	$0.80\ \lambda_g \times 0.57\ \lambda_g$
[25]	Ethanol	0%, 10%, 30%, 50%, 70%, 90%, 100%	Complementary split-ring resonator (CSRR)	Rogers RO3035	Yes	2.3 GHz	~ 150 MHz	~ 1.5 MHz	N/A	~ 0.0021	N/A	$0.29\ \lambda_g \times 0.4\ \lambda_g$
[26]	Methanol	0–100% step size of 10%	Step impedance resonator (SIR)	Rogers RT6002	Yes	1.91 GHz	~ 500 MHz	~ 5 MHz	N/A	~ 0.0098	4.5%	$0.11\ \lambda_g \times 0.34\ \lambda_g$
[52]	Ethanol	5-35% step size of 5%	Meander structure (MS), Ladder structure (LS), and T-structure (TS)	Rogers 4003	No	3 GHz	~ 1.1 GHz	~ 36.67 MHz	3,500	~ 0.0611	0.11 %	$0.1\ \lambda_g \times 1.3\ \lambda_g$
This Work	**Ethanol**	**65–75% step size of 1%**	**Modified Jerusalem Resonator**	**Rogers RT/Duroid 5880**	**Yes**	**5.58 GHz**	**14.10 MHz**	**1.41 MHz**	**279**	**0.2014 MHz**	**0.69 %**	**$0.28\ \lambda_g \times 0.56\ \lambda_g$**
	Methanol	**65–75% step size of 1%**					**19.54 MHz**	**1.95 MHz**	**279**	**0.3908 MHz**	**1.81 %**	

the resonant frequency shifted to 5.4950 GHz at 75% methanol. The measurement bandwidth was 19.54 MHz. The sensor's sensitivity to the percentage of methanol in the aqueous solution can be determined as the ratio between the bandwidth of methanol and the bandwidth of the difference in resonant frequencies, that is, the slope of the transfer function shown in Figure 12 (gray dashed line). The sensitivity of methanol concentration in the range of 65 to 75% is 1.95 MHz per % methanol.

Regarding ethanol in the aqueous solutions, the lowest resonant frequency was observed at a low ethanol concentration of 65%, with a resonant frequency of 5.505 GHz. The trend of the graph is similar to that of methanol concentration in the aqueous solutions. The highest resonant frequency was observed at 5.5191 GHz when the ethanol concentration was 75%. The bandwidth range was 14.1 MHz. The linear curve fitting is shown in Figure 12 (black dashed line). The sensitivity of ethanol concentration in the range of 65 to 75% was found to be 1.41 MHz per % ethanol.

Overall, the operating frequency range for methanol (green zone) does not overlap with that for ethanol (yellow zone). Thus, the proposed sensor can discriminate the percentage in the range of 65 to 75% and the type of alcohol, whether ethanol-based or methanol-based, from a single measurement.

Table 4 provides a comprehensive comparison of the sensors utilized in this study with those from other published works, focusing on various crucial parameters. These parameters include measurement technique, operating frequency, maximum sensing bandwidth, sensitivity,

Q-Factor, frequency detection resolution (FDR) [13], measurement error, as well as details regarding the material substrate and the dimensions of the sensor.

E. SENSOR REPRODUCIBILITY

To evaluate the reproducibility of the proposed sensor, two experiments were conducted. Firstly, methanol liquid-mixtures were injected three times without any changes to the system setup. The standard deviation of these measurements was then calculated, resulting in minimum, maximum, and average values of 0.0026, 0.0682, and 0.0326, respectively, for the measured reflection coefficient, S_{11}. Then, the liquid samples were replaced with ethanol liquid-mixtures, and a similar procedure was carried out. The minimum, maximum, and average standard deviations of the measured reflection coefficient, S_{11}, were calculated to be 0.0041, 0.0716, and 0.0434, respectively.

Secondly, the sensor was removed and re-mounted at SMA port, and the measurement was repeated three times. For this second experiment with the methanol liquid-mixture, the minimum, maximum, and average standard deviations of the measured reflection coefficient, S_{11}, were calculated to be 0.0035, 0.0764, and 0.0447, respectively. Subsequently, for the experiment with the ethanol liquid-mixture, the minimum, maximum, and average standard deviations of the measured reflection coefficient, S_{11}, were calculated to be 0.0048, 0.0831, and 0.0496, respectively.

Based on the measured results and analytical data, it is evident that the error of the sensor increases when re-installing the systematic measurements for both types of alcohols. However, to mitigate measurement error, several strategies can be employed. These include ensuring secure locking of all positions, particularly in the sensing area. Furthermore, it is imperative for the sensor to exhibit a high Q-factor and a deep resonance of reflection coefficients, S_{11}, [12].

IV. POTENTIAL APPLICATIONS

Ethanol and isopropyl alcohol serve as disinfectants due to their effectiveness against various bacteria, viruses, and fungi. The biocidal efficacy of these alcohols relies significantly on their concentration and hydrophilic properties, with the optimal antimicrobial activity falling within the 60–80% alcohol concentration range. Lower concentrations are ineffective against the virus, while higher alcohol concentrations can adversely affect human skin.

Two challenges persist in verifying disinfectant solutions. Firstly, there is the issue of determining the percentage of ethanol in the disinfectant. Methanol should not be mixed into the COVID-19 disinfectant because it is not of food-grade quality. Second, there is the challenge of correctly identifying the type of alcohol used, such as distinguishing between ethanol and methanol, when mixing solutions for disinfection.

A modified Jerusalem liquid mixture sensor was developed as a non-destructive sensor to discriminate the type and percentage of alcohol in disinfectants against COVID-19. The evaluation focused on two conditions: alcohol type and concentration. The modified Jerusalem sensor effectively distinguished between ethanol and methanol in aqueous solutions, with a 16 MHz frequency difference. To prioritize disinfectant efficacy against COVID-19, we tested alcohol percentages from 65 to 75% in 1% increments.

V. CONCLUSION

This research introduces a flat microwave sensor intended for identifying the type and concentration of alcohol within water-based solutions. The sensor was developed by adapting the Jerusalem patch to amplify the electrical field strength and reduce its physical size. Operating at a frequency of 5.88 GHz within the ISM band, which is a balance between sensitivity and cost-effectiveness. Utilizing 3D printing technology, a custom case was created to securely house the modified Jerusalem sensor and feeding tube, minimizing measurement errors. The sensor's performance was assessed based on two conditions: alcohol type and concentration. Successfully distinguishing between ethanol and methanol in water-based solutions, the modified Jerusalem sensor displayed a frequency gap of 16 MHz between the two substances,

ensuring non-overlapping frequency spectra. For alcohol percentages between 65–75%, an increase of 1% was maintained to address the application of disinfectants against COVID-19. The gathered data facilitated the development of a mathematical model to determine ethanol and methanol concentrations in water-based solutions, with the proposed sensor exhibiting a maximum error of less than 1.81%. This adapted Jerusalem sensor offers numerous advantages, including its non-invasive nature, suitability for real-time monitoring, and absence of life-cycle constraints.

REFERENCES

[1] (2023). *World Health Organization, Coronavirus Disease (COVID-19) Pandemic*. Accessed: Jan. 10, 2023. [Online]. Available: https://www.who.int/emergencies/diseases/novel-coronavirus-2019

[2] H. Kweon, J.-W. Choi, and S.-Y. Yoon, "Analysis of consumer exposure cases for alcohol-based disinfectant and hand sanitizer use against coronavirus disease 2019 (COVID-19)," *Int. J. Environ. Res. Public Health*, vol. 19, no. 1, p. 100, Dec. 2021, doi: 10.3390/ijerph19010100.

[3] M. Neufeld, D. W. Lachenmeier, C. Ferreira-Borges, and J. Rehm, "Is alcohol an 'essential goo' during COVID-19? Yes, but only as a disinfectant!" *Alcoholism, Clin. Experim. Res.*, vol. 44, no. 9, pp. 1906–1909, Sep. 2020, doi: 10.1111/acer.14417.

[4] K. Abuga and N. Nyamweya, "Alcohol-based hand sanitizers in COVID-19 prevention: A multidimensional perspective," *Pharmacy*, vol. 9, no. 1, p. 64, Mar. 2021, doi: 10.3390/pharmacy9010064.

[5] A. Berardi, D. R. Perinelli, H. A. Merchant, L. Bisharat, I. A. Basheti, G. Bonacucina, M. Cespi, and G. F. Palmieri, "Hand sanitisers amid COVID-19: A critical review of alcohol-based products on the market and formulation approaches to respond to increasing demand," *Int. J. Pharmaceutics*, vol. 584, Jun. 2020, Art. no. 119431, doi: 10.1016/j.ijpharm.2020.119431.

[6] A. Ebrahimi, W. Withayachumnankul, S. Al-Sarawi, and D. Abbott, "High-sensitivity metamaterial-inspired sensor for microfluidic dielectric characterization," *IEEE Sensors J.*, vol. 14, no. 5, pp. 1345–1351, May 2014, doi: 10.1109/JSEN.2013.2295312.

[7] C.-S. Lee and C.-L. Yang, "Complementary split-ring resonators for measuring dielectric constants and loss tangents," *IEEE Microw. Wireless Compon. Lett.*, vol. 24, no. 8, pp. 563–565, Aug. 2014, doi: 10.1109/LMWC.2014.2318900.

[8] Y. Seo, M. U. Memon, and S. Lim, "Microfluidic eighth-mode substrate-integrated-waveguide antenna for compact ethanol chemical sensor application," *IEEE Trans. Antennas Propag.*, vol. 64, no. 7, pp. 3218–3222, Jul. 2016, doi: 10.1109/TAP.2016.2559581.

[9] S. Kayal, T. Shaw, and D. Mitra, "Design of metamaterial based compact and highly sensitive microwave liquid sensor," *Appl. Phys. A*, vol. 13, no. 1, pp. 1–9, 2019.

[10] A. Salim and S. Lim, "Complementary split-ring resonator-loaded microfluidic ethanol chemical sensor," *Sensors*, vol. 16, no. 11, p. 1802, Oct. 28, 2016, doi: 10.3390/s16111802.

[11] S. Kiani, P. Rezaei, and M. Fakhr, "Dual-frequency microwave resonant sensor to detect noninvasive glucose-level changes through the fingertip," *IEEE Trans. Instrum. Meas.*, vol. 70, pp. 1–8, 2021, doi: 10.1109/TIM.2021.3052011.

[12] S. Kiani, P. Rezaei, M. Navaei, and M. S. Abrishamian, "Microwave sensor for detection of solid material permittivity in single/multilayer samples with high quality factor," *IEEE Sensors J.*, vol. 18, no. 24, pp. 9971–9977, Dec. 2018, doi: 10.1109/JSEN.2018.2873544.

[13] S. Kiani, P. Rezaei, and M. Fakhr, "Real-time measurement of liquid permittivity through label-free meandered microwave sensor," *IETE J. Res.*, vol. 1, pp. 1–11, Jul. 2023, doi: 10.1080/03772063.2023.2231875.

[14] S. Kiani and P. Rezaei, "Microwave substrate integrated waveguide resonator sensor for non-invasive monitoring of blood glucose concentration: Low cost and painless tool for diabetics," *Measurement*, vol. 219, Sep. 2023, Art. no. 113232, doi: 10.1016/j.measurement.2023.113232.

[15] S. Kiani, P. Rezaei, and M. Navaei, "Dual-sensing and dual-frequency microwave SRR sensor for liquid samples permittivity detection," *Measurement*, vol. 160, Aug. 2020, Art. no. 107805, doi: 10.1016/j.measurement.2020.107805.

[16] H. Nimehvari Varcheh, P. Rezaei, and S. Kiani, "A modified Jerusalem microstrip filter and its complementary for low phase noise X-band oscillator," *Int. J. Microw. Wireless Technol.*, vol. 15, no. 10, pp. 1707–1716, Dec. 2023, doi: 10.1017/s1759078723000703.

[17] S. Kiani, P. Rezaei, and M. Fakhr, "Investigation of microwave resonant sensors for use in detecting changes of noninvasive blood glucose concentration," in *Organic and Inorganic Materials Based Sensors*. Hoboken, NJ, USA: Wiley, 2023, pp. 1055–1064, doi: 10.1002/9783527834266.ch45.

[18] E. Silavwe, N. Somjit, and I. D. Robertson, "A microfluidic-integrated SIW lab-on-substrate sensor for microliter liquid characterization," *IEEE Sensors J.*, vol. 16, no. 21, pp. 7628–7635, Nov. 1, 2016, doi: 10.1109/JSEN.2016.2599099.

[19] P. Vélez, L. Su, K. Grenier, J. Mata-Contreras, D. Dubuc, and F. Martín, "Microwave microfluidic sensor based on a microstrip splitter/combiner configuration and split ring resonators (SRRs) for dielectric characterization of liquids," *IEEE Sensors J.*, vol. 17, no. 20, pp. 6589–6598, Oct. 2017, doi: 10.1109/JSEN.2017.2747764.

[20] N. Jankovic and V. Radonic, "A microwave microfluidic sensor based on a dual-mode resonator for dual-sensing applications," *Sensors*, vol. 17, no. 12, p. 2713, Nov. 24, 2017, doi: 10.3390/s17122713.

[21] N. Chudpooti, E. Silavwe, P. Akkaraekthalin, I. D. Robertson, and N. Somjit, "Nano-fluidic millimeter-wave lab-on-a-waveguide sensor for liquid-mixture characterization," *IEEE Sensors J.*, vol. 18, no. 1, pp. 157–164, Jan. 2018, doi: 10.1109/JSEN.2017.2772348.

[22] N. Chudpooti, V. Doychinov, P. Akkaraekthalin, I. D. Robertson, and N. Somjit, "Non-invasive millimeter-wave profiler for surface height measurement of photoresist films," *IEEE Sensors J.*, vol. 18, no. 8, pp. 3174–3182, Apr. 2018, doi: 10.1109/JSEN.2018.2806185.

[23] M. Abdolrazzaghi, M. Daneshmand, and A. K. Iyer, "Strongly enhanced sensitivity in planar microwave sensors based on metamaterial coupling," *IEEE Trans. Microw. Theory Techn.*, vol. 66, no. 4, pp. 1843–1855, Apr. 2018, doi: 10.1109/TMTT.2018.2791942.

[24] N. Chudpooti, V. Doychinov, B. Hong, P. Akkaraekthalin, I. Robertson, and N. Somjit, "Multi-modal millimeter-wave sensors for plastic polymer material characterization," *J. Phys. D, Appl. Phys.*, vol. 51, no. 27, Jun. 18, 2018, Art. no. 275103, doi: 10.1088/1361-6463/aac818.

[25] E. L. Chuma, Y. Iano, G. Fontgalland, and L. L. Bravo Roger, "Microwave sensor for liquid dielectric characterization based on metamaterial complementary split ring resonator," *IEEE Sensors J.*, vol. 18, no. 24, pp. 9978–9983, Dec. 2018, doi: 10.1109/JSEN.2018.2872859.

[26] A. Ebrahimi, J. Scott, and K. Ghorbani, "Ultrahigh-sensitivity microwave sensor for microfluidic complex permittivity measurement," *IEEE Trans. Microw. Theory Techn.*, vol. 67, no. 10, pp. 4269–4277, Oct. 2019, doi: 10.1109/TMTT.2019.2932737.

[27] W. Krudpun, N. Chudpooti, P. Lorwongtragool, S. Seewattanapon, and P. Akkaraekthalin, "PSE-coated interdigital resonator for selective detection of ammonia gas sensor," *IEEE Sensors J.*, vol. 19, no. 23, pp. 11228–11235, Dec. 2019, doi: 10.1109/JSEN.2019.2936102.

[28] N. Chudpooti, N. Duangrit, P. Sangpet, P. Akkaraekthalin, B. U. Imberg, I. D. Robertson, and N. Somjit, "In-situ self-aligned NaCl-solution fluidic-integrated microwave sensors for industrial and biomedical applications," *IEEE Access*, vol. 8, pp. 188897–188907, 2020, doi: 10.1109/ACCESS.2020.3031864.

[29] A. Javed, A. Arif, M. Zubair, M. Q. Mehmood, and K. Riaz, "A low-cost multiple complementary split-ring resonator-based microwave sensor for contactless dielectric characterization of liquids," *IEEE Sensors J.*, vol. 20, no. 19, pp. 11326–11334, Oct. 2020, doi: 10.1109/JSEN.2020.2998004.

[30] O. Niksan, M. C. Jain, A. Shah, and M. H. Zarifi, "A nonintrusive flow rate sensor based on microwave split-ring resonators and thermal modulation," *IEEE Trans. Microw. Theory Techn.*, vol. 70, no. 3, pp. 1954–1963, Mar. 2022, doi: 10.1109/TMTT.2022.3142038.

[31] D. Prakash and N. Gupta, "High-sensitivity grooved CSRR-based sensor for liquid chemical characterization," *IEEE Sensors J.*, vol. 22, no. 19, pp. 18463–18470, Oct. 2022, doi: 10.1109/JSEN.2022.3198837.

[32] A. Pourafzal, T. Roi-Taravella, M. Cheffena, and S. Y. Yayilgan, "A low-cost and accurate microwave sensor system for permittivity characterization," *IEEE Sensors J.*, vol. 23, no. 2, pp. 1234–1248, Jan. 2023, doi: 10.1109/JSEN.2022.3225662.

[33] A. Secme, U. Tefek, B. Sari, H. S. Pisheh, H. D. Uslu, Ö. A. Çaliskan, B. Kucukoglu, R. T. Erdogan, H. Alhmoud, O. Sahin, and M. S. Hanay, "High-resolution dielectric characterization of single cells and microparticles using integrated microfluidic microwave sensors," *IEEE Sensors J.*, vol. 23, no. 7, pp. 6517–6529, Apr. 2023, doi: 10.1109/JSEN.2023.3250401.

[34] M. Palandoken, C. Gocen, T. Khan, Z. Zakaria, I. Elfergani, C. Zebiri, J. Rodriguez, and R. A. Abd-Alhameed, "Novel microwave fluid sensor for complex dielectric parameter measurement of ethanol–water solution," *IEEE Sensors J.*, vol. 23, no. 13, pp. 14074–14083, Jul. 2023, doi: 10.1109/JSEN.2023.3276817.

[35] D. Prakash and N. Gupta, "Microwave grooved SRR sensor for detecting low concentration ethanol-blended petrol," *IEEE Sensors J.*, vol. 23, no. 14, pp. 15544–15551, Jul. 2023, doi: 10.1109/JSEN.2023.3279851.

[36] N. Chudpooti, N. Duangrit, and P. Akkaraekthalin, "A miniaturized planar sensor using Minkowski fractal technique for material characterization," in *Proc. 16th Int. Conf. Electr. Eng. Electron., Comput., Telecommun. Inf. Technol. (ECTI-CON)*, Jul. 2019, pp. 756–759, doi: 10.1109/ECTI-CON47248.2019.8955132.

[37] N. Chudpooti, P. Sangpet, N. Duangrit, P. Akkaraekthalin, I. D. Robertson, and N. Somjit, "An integrated 3D-printed lens with ultra-wideband flower-shaped stub antenna for ethanol-water mixture characterization," in *Proc. Res., Invention, Innov. Congr., Innov. Electricals Electron. (RI2C)*, Sep. 2021, pp. 80–83, doi: 10.1109/RI2C51727.2021.9559770.

[38] R. A. Alahnomi, Z. Zakaria, Z. M. Yussof, A. A. Althuwayb, A. Alhegazi, H. Alsariera, and N. A. Rahman, "Review of recent microwave planar resonator-based sensors: Techniques of complex permittivity extraction, applications, open challenges and future research directions," *Sensors*, vol. 21, no. 7, p. 2267, Mar. 2021, doi: 10.3390/s21072267.

[39] E. L. Chuma and Y. Iano, "Novelty sensor using integrated fluorescence and dielectric spectroscopy to improve food quality identification," *IEEE Sensors*, vol. 1, no. 1, pp. 1–4, Aug. 2022.

[40] E. L. Chuma and T. Rasmussen, "Metamaterial-based sensor integrating microwave dielectric and near-infrared spectroscopy techniques for substance evaluation," *IEEE Sensors J.*, vol. 22, no. 20, pp. 19308–19314, Oct. 2022, doi: 10.1109/JSEN.2022.3202708.

[41] M. Navaei, P. Rezaei, and S. Kiani, "A symmetric bar chart-shape microwave sensor with high Q-factor for permittivity determination of fluidics," *Int. J. Microw. Wireless Technol.*, vol. 15, no. 8, pp. 1334–1342, Oct. 2023, doi: 10.1017/s1759078723000053.

[42] *Computer Simulation Technology*, CST-MW Studio, Framingham, MA, USA, 2017.

[43] M. Hosseinipanah and Q. Wu, "Equivalent circuit model for designing of Jerusalem cross-based artificial magnetic conductors," *Radioengineering*, vol. 18, no. 4, pp. 544–550, 2029.

[44] *RT/Duriod 5870–5880 Datasheet*. Accessed: May 1, 2023. [Online]. Available: https://www.rogerscorp.com/advanced-electronics-solutions/rt-duroid-laminates/rt-duroid-5880-laminates

[45] H. R. Heidari, P. Rezaei, S. Kiani, and M. Taherinezhad, "A monopulse array antenna based on SIW with circular polarization for using in tracking systems," *AEU-Int. J. Electron. Commun.*, vol. 162, Apr. 2023, Art. no. 154563, doi: 10.1016/j.aeue.2023.154563.

[46] D. Lim, S. Yu, and S. Lim, "Miniaturized metamaterial absorber using three-dimensional printed stair-like Jerusalem cross," *IEEE Access*, vol. 6, pp. 43654–43659, 2018, doi: 10.1109/ACCESS.2018.2862160.

[47] C. Hua, R. Li, Y. Wang, and Y. Lu, "Dual-polarized filtering antenna with printed jerusalem-cross radiator," *IEEE Access*, vol. 6, pp. 9000–9005, 2018, doi: 10.1109/ACCESS.2018.2803790.

[48] H.-Y. Chen and Y. Tao, "Performance improvement of a U-Slot patch antenna using a dual-band frequency selective surface with modified Jerusalem cross elements," *IEEE Trans. Antennas Propag.*, vol. 59, no. 9, pp. 3482–3486, Sep. 2011, doi: 10.1109/TAP.2011.2161440.

[49] *LPKF. Specification and Operational Characteristics of LPKF ProtoMat S100*. Accessed: May 8, 2023. [Online]. Available: http://www.spezial.cz/pdf/protomat_s100.pdf

[50] *User Manual PHOTON ULTRA*. Accessed: Apr. 13, 2023. [Online]. Available: http://efaidnbmnnnibpcajpcglclefindmkaj

[51] (2023). *Product Description: Colored UV Resin 1KG*. Accessed: Apr. 13, 2023. [Online]. Available: https://www.anycubic.com/

[52] M. Navaei, P. Rezaei, and S. Kiani, "Measurement of low-loss aqueous solutions permittivity with high detection accuracy by a contact and free-label resonance microwave sensor," *Int. J. Commun. Syst.*, vol. 36, no. 5, pp. 1–24, Dec. 2022, doi: 10.1002/dac.5417.

NONCHANUTT CHUDPOOTI (Member, IEEE) received the B.Sc. degree (Hons.) in industrial physics and medical instrumentation and the Ph.D. degree in electrical engineering from the King Mongkut's University of Technology North Bangkok, Bangkok, Thailand, in 2012 and 2018, respectively.

He was a Lecturer with the Department of Industrial Physics and Medical Instrumentation, Faculty of Applied Science, in 2018. His research interests include the application of microwave microfluidic sensors, millimeter-wave substrate integrated circuit applications, substrate-integrated waveguide applications, and 3D printing technologies.

Dr. Chudpooti has been a member of the Electrical Engineering/Electronics, Computer, Telecommunications, and Information Technology (ECTI), Thailand, since 2020. He was appointed as a ECTI Board Committee Member, from 2020 to 2023. He was a recipient of the Best Presentation Award from Thailand–Japan Microwave, in 2015 and 2018, and the Young Researcher Encouragement Award, in 2016. Currently, he is an Associate Editor of *ECTI Transactions on Electrical Engineering, Electronics, and Communications* and an Editor of *Journal of Applied Science and Emerging Technology*.

TANAPORN PECHRKOOL was born in Chumphon, Thailand, in 1987. He received the B.Eng. degree in electronics and telecommunications engineering from the Rajamangala University of Technology Phra Nakhon, in 2010, the M.Eng. degree in electrical engineering from the King Mongkut's University of Technology North Bangkok (KMUTNB), Thailand, in 2014. He is currently pursuing the Ph.D. degree with the Department of Electrical and Computer Engineering. He is a Lecturer with the Faculty of Engineering, Rajamangala University of Technology Thanyaburi. His research interests include microwave sensors, ZOR antenna, and telecommunication.

PATCHADAPORN SANGPET was born in Chiang Rai, Thailand, in 1992. She received the bachelor's degree in industrial physics and medical equipment, the master's degree in electrical and computer engineering, and the Ph.D. degree in electrical engineering from the King Mongkut's University of Technology North Bangkok (KMUTNB), Bangkok, Thailand, in 2013, 2016, and 2023, respectively.

Her research interests include ultra-wideband antenna, microwave sensors, and 3D-printed for its applications.

PRAYOOT AKKARAEKTHALIN (Member, IEEE) received the B.Eng. and M.Eng. degrees in electrical engineering from the King Mongkut's University of Technology North Bangkok (KMUTNB), Bangkok, Thailand, in 1986 and 1990, respectively, and the Ph.D. degree from the University of Delaware, Newark, DE, USA, in 1998.

From 1986 to 1988, he was a Research and Development Engineer with Microtek Products Company Ltd., Thailand. In 1988, he joined the Department of Electrical Engineering, KMUTNB. He was the Head of the Senior Research Scholar Project, which is supported by Thailand Research Fund, from 2015 to 2017. He has authored or co-authored more than 40 international journals, 200 conference papers, and four books/book chapters. His current research interests include RF/microwave circuits, wideband and multiband antennas, telecommunication, and sensor systems.

Dr. Akkaraekthalin is a member of the Institute of Electronics, Information and Communication Engineers (IEICE), Japan; the Electrical Engineering/Electronics, Computer, Telecommunications, and Information Technology (ECTI); and the Electrical Engineering Academic Association (EEAAT), Thailand. He was the Chairperson of the IEEE Microwave Theory and Techniques/Antennas and Propagation/Electron Devices (MTT/AP/ED) Thailand Joint Chapter, from 2007 to 2010; and the Vice President and the President of the ECTI Association, Thailand, from 2012 to 2013 and from 2014 to 2015, respectively. He was the Editor-in-Chief of *ECTI Transactions*, from 2011 to 2013.

IAN D. ROBERTSON (Fellow, IEEE) received the B.Sc. (Eng.) and Ph.D. degrees from King's College London, London, U.K., in 1984 and 1990, respectively.

From 1984 to 1986, he was with the GaAs MMIC Research Group, Plessey Research, Caswell, U.K. Then, he returned to King's College London, initially as a Research Assistant working on the T-SAT Project and then as a Lecturer leading the MMIC Research Team, where he became a Reader, in 1994. In 1998, he was a Professor of microwave subsystems engineering with the University of Surrey, Guildford, U.K., where he established the Microwave Systems Research Group and was a Founding Member of the Advanced Technology Institute. In 2004, he was appointed to the Centenary Chair in microwave and millimeter-wave circuits with the University of Leeds, Leeds, U.K. He was the Director of Learning and Teaching, from 2006 to 2011, and the Head of the School, from 2011 to 2016.

Dr. Robertson was the General Technical Program Committee Chair of European Microwave Week, in 2011 and 2016.

NUTAPONG SOMJIT (Senior Member, IEEE) received the Dipl.Ing. (M.Sc.) degree from Dresden University of Technology, in 2005, and the Ph.D. degree from the KTH Royal Institute of Technology, in 2012. Then, he returned to Dresden University of Technology to lead a Research Team in Micro-Sensors and MEMS ICs for the Chair for Circuit Design and Network Theory. In 2013, he was appointed as a Lecturer (an Assistant Professor) with the School of Electronic and Electrical Engineering, University of Leeds, where he is currently an Associate Professor. Since 2022, he has been appointed to lead the Research Team as an Adjunct Faculty Member with the Micro and Nanosystems Department, KTH Royal Institute of Technology. Since 2024, he has been with Shaoxing University, China, as a Full Research Professor. His research interests include integrated smart high-frequency components, heterogeneous integration, and low-cost microfabrication processes. He was a recipient of the Best Paper Award (EuMIC Prize) at European Microwave Week, in 2009. He was awarded a Graduate Fellowship from the IEEE Microwave Theory and Techniques Society (MTT-S), in 2010 and 2011, and the IEEE Doctoral Research Award from the IEEE Antennas and Propagation Society, in 2012. In 2016, he was the Chair of the Student Design Competition for the European Microwave Week. In 2018, he was appointed as an Associate Editor of *Electronics Letters*.